Case Studies in Thermal Engineering 59 (2024) 104585

Contents lists available at ScienceDirect

Case Studies in Thermal Engineering

journal homepage: www.elsevier.com/locate/csite

A novel thermal management system **for** a cylindrical battery based on tubular thermoelectric generator

Xiao Zhou [a], Azher M Abed [b,c,**], Rishabh Chaturvedi [d,***], Barno Sayfutdinovna Abdullaeva [e], Ali Shawabkeh [f], Yasser Fouad [g,*], Fahid Riaz [h,****]

[a] School of Mathematics, Physics and Optoelectronic Engineering, Hubei University of Automotive Technology, Shiyan, 442000, Hubei, China
[b] Air Conditioning and Refrigeration Techniques Engineering Department, College of Engineering and Technologies, Al-Mustaqbal University, Babylon, 51001, Iraq
[c] Al - Mustaqbal Center for Energy Research, Al-Mustaqbal University, Babylon, 51001, Iraq
[d] Department of Mechanical Engineering, GLA University, Mathura, India
[e] Department of Mathematics and Information Technologies, Vice-Rector for Scientific Affairs, Tashkent State Pedagogical University, Tashkent, Uzbekistan
[f] College of Engineering and Technology, American University of the Middle East, Kuwait
[g] Department of Applied Mechanical Engineering, College of Applied Engineering, Muzahimiyah Branch, King Saud University, Saudi Arabia
[h] College of Engineering, Abu Dhabi University, Abu Dhabi, United Arab Emirates

A R T I C L E I N F O

Keywords:
Battery thermal management
Waste heat recovery
Tubular thermoelectric generator
Cylindrical lithium-ion battery

A B S T R A C T

This study introduces an innovative thermal management system tailored for cylindrical Lithium-ion batteries. It integrates a tubular thermoelectric generator (TTEG) to handle both battery thermal management and the utilization of waste heat for power generation. The main focus lies in evaluating the waste heat recovery capabilities of the TTEG to enhance effective thermal management. The research investigates key geometric and operational parameters such as battery discharge rate (C-rate), thermocouple count (NTC), heat transfer coefficient (HTC), and thermoelectric leg height (HL) to comprehensively assess the overall system performance. The results highlight that integrating the TTEG improves thermal management and waste heat recovery in lithium-ion batteries. It demonstrates temperature reductions of up to 21 °C at a discharge rate of 3C compared to batteries without the TTEG thermal management system. Additionally, increasing the NTC leads to a rise in the maximum battery temperature, thereby enhancing waste heat recovery performance. For instance, increasing the number of thermocouples from 100 to 144 results in a substantial up to 70 % increase in TTEG voltage.Furthermore, enhancing HTC and HL positively impacts thermal performance, showing a significant decrease in the maximum battery temperature. Elevated HTC and HL also contribute to improving thermoelectric voltage, power, and conversion efficiency, highlighting their dual role in enhancing waste heat recovery. For instance, at peak conditions, there is a notable reduction of 2.66 °C in the maximum battery temperature with an HL of 12 mm compared to 4 mm. Additionally, increasing HTC from 10 to

* Corresponding author.
** Corresponding author.
*** Corresponding author.
**** Corresponding author.
E-mail addresses: azhermuhson@uomus.edu.iq (A. M Abed), rishabh.chaturvedi@gla.ac.in (R. Chaturvedi), yfouad@ksu.edu.sa (Y. Fouad), fahid.riaz@adu.ac.ae (F. Riaz).

https://doi.org/10.1016/j.csite.2024.104585
Received 19 February 2024; Received in revised form 6 May 2024; Accepted 18 May 2024
Available online 21 May 2024

20, particularly at maximum discharge, leads to a surge of 15.87 % in voltage and a substantial 34.28 % increase in output power.

Nomenclature

c_p	specific heat at constant pressure, $\left(Jkg^{-1}K^{-1}\right)$
E	electric field intensity, $\left(Vm^{-1}\right)$
I	electric current, (A)
I_b	discharge current of battery, (A)
J	electric current density, $\left(Am^{-2}\right)$
L	device length, (mm)
M	number of rings
N	number of thermocouples in each ring
P_{TEG}	thermoelectric power output, (W)
Q	heat source, (W)
Q_b	generated heat in the lithium-ion battery, (W)
Q_h	heat absorbed by thermoelectric, (W)
R	electrical resistivity, (Ωm)
R_{TEG}	internal resistance of the thermoelectric, (Ωm)
r_b	radius of cylindrical battery, (mm)
R_b	internal resistance of the battery, (Ωm)
R_L	load resistance, (Ω)
h	height, (mm)
h_{cr}	ceramics height, (mm)
h_{ic}	interconnectors height, (mm)
S	Seebeck coefficient, $\left(VK^{-1}\right)$
T	temperature, (K)
T_{max}	maximum temperature of battery, (K)
V	voltage, (V)
$V_{oc,b}$	open circuit voltage of battery, (V)
V_{TEG}	open circuit voltage of thermoelectric, (V)
V_b	volume of battery, $\left(m^3\right)$

Greek letters

α	Seebeck coefficient, $\left(VK^{-1}\right)$
η_{TTEG}	conversion efficiency thermoelectric generator
Δ	difference
λ	thermal conductivity, $\left(Wm^{-2}K^{-1}\right)$
ρ	density, $\left(kgm^{-3}\right)$
σ	electrical conductivity, (Sm)

Abbreviations

BMS	battery management system
BTMS	battery thermal management system
EV	electric vehicle
HL	height of PN legs, (mm)
HTC	heat transfer coefficient, $\left(Wm^{-2}K^{-1}\right)$
LI	lithium-ion
LIB	lithium-ion battery
NTC	number of thermocouples
PCM	phase change material
TEG	thermoelectric generator
TTEG	tubular annular thermoelectric generator

1. Introduction

With the rise in global energy demand and escalating environmental damage caused by fossil fuel consumption, the quest for eco-friendly, renewable energy sources has become increasingly pressing [1].In the current movement towards emission-free electrification, batteries serve as a crucial component in energy storage [2–4]. The advent of commercial lithium-ion batteries (LIBs) in the early 1990s marked a transformative milestone, establishing them as the preferred option for various applications, including mobile phones, electric vehicles (EVs), and drones. With recent advancements in electrification, lithium-ion batteries have become extensively utilized in electric and hybrid vehicles [5,6]. Thanks to recent technological advancements in electric motors and lithium batteries, electric pump-fed engines are now being explored as an alternative to conventional engines reliant on pressurized or turbopumps [7–9]. Li-ion batteries stand out due to their highest energy density, minimal self-discharge rates, and extended service life, distinguishing them from other rechargeable technologies [10]. However, this technology is not without thermal drawbacks. Specifically, under discharge conditions, redox reactions within the battery generate a substantial amount of heat, leading to an excessive rise in battery temperature. Many researchers investigated the electrical and thermal behavior of batteries using numerical and experimental approaches [11–15]. Consequently, the development of a battery cooling system is imperative to prevent potential cell damage from elevated operational temperatures [16]. To address this issue, integrating a battery management system (BMS) in Li-ion batteries is a viable solution. The BMS monitors the battery's regular functioning and optimizes its operation. Thermal management involves efficiently controlling heat within electronic or mechanical devices to guarantee their regular operation and long-term stability [17]. Various approaches, including active, passive, and hybrid methods, have been suggested for the thermal management of batteries. Nevertheless, a significant amount of heat is dissipated as waste during battery operation [18]. Najafi Khaboshan et al. [19] examined configurations of battery thermal management systems (BTMS) involving fins, metal foam, and phase change material (PCM) to reduce battery temperatures. Patil et al. [20] examined the thermal performance of water-cooled lithium-ion battery cells and packs used in electric vehicles under high discharge rates using a U-turn type microchannel cold plate. Talele et al. [21] explored a strategy for delaying battery thermal runaway using various phase change materials with different melting points. Zhu et al. [22] conducted a computational investigation into a battery thermal management system employing nano-enhanced phase change material under hot climate conditions. On the other hand, the thermoelectric effect shows promise for power generation and refrigeration. It enables converting waste heat from industrial processes into electricity via thermoelectric generators [23]. Therefore, implementing a thermoelectric generator waste heat recovery system in a battery system can manage thermal conditions and harness power from the waste heat generated within the battery. The subsequent section summarizes the latest studies in employing thermoelectric conversion technologies within battery systems.

Lyu et al. [24] conducted an experimental investigation into the utilization of thermoelectric conversion technologies, specifically integrating forced air cooling and liquid cooling methods, to manage the thermal conditions of batteries in electric vehicles. The experimental results indicate a significant reduction of approximately 43 °C in the battery surface temperature when employing a thermoelectric-based water-cooling system for a singular cell equipped with a copper holder, under the application of 40 V to the heater and 12 V to the thermoelectric module. Li et al. [25] developed a coupled electro-thermal model of a 30Ah prismatic LIB. They calibrated it via hybrid pulse power, charge-discharge, time-temperature, and resistance tests to accurately predict battery performance. Alhumade et al. [26] numerically studied non-Newtonian hybrid nano-coolants and thermoelectric cooling for LIBs, varying flow geometry. Inlet Reynolds numbers of 200–800 were tested for non-Newtonian fluids with 0.05–0.5 % volume fractions to estimate heatsink, battery, and thermoelectric hot side temperatures. Results showed nanoparticles increased ΔP by 267 % and 95 % at Re = 20 and 800, respectively. Jiang et al. [27] experimentally studied a cylindrical battery module with phase change material composite under thermoelectric cooling. They examined transient and steady-state thermal behaviors, contrasting thermoelectric cooling with natural convection and liquid cooling. Thermoelectric cooling significantly reduced battery temperature and extended operating time compared to the other methods. Liao et al. [28] created a hybrid thermal management system for LIBs using thermoelectric elements and phase change materials to enable operation in extreme environments. The composite PCM and thermoelectric elements together limited maximum battery temperature below 318.15 K during 3C discharging in hot conditions. The module's maximum internal temperature differential was kept around 3K. Lyu et al. [29] experimentally investigated a novel battery pack design incorporating acrylic casing, copper holders, liquid cooling, and battery cells. In the 40 V test scenario, the implemented system demonstrated a temperature reduction of approximately 20 °C in comparison to a setup employing solely liquid cooling. Tu et al. [30] experimentally studied the thermal-hydraulic and power generation performance of a waste heat recovery device for batteries. The study analyzed the effects of groove design and nanofluid concentration on heat transfer and power generation of the battery waste heat recovery device. Cui et al. [31] developed a robust predictive thermal management strategy for batteries using thermoelectric cooling, accounting for thermal resistance. The method effectively adjusted battery temperature within an optimal range, minimizing energy consumption. Experiments demonstrated its accuracy in maintaining the battery near target temperatures across various cycles, with errors consistently below 0.5 °C. Shi et al. [32] created a lumped thermoelectric coupling model for batteries incorporating multi-timescale dynamics. Their novel multi-feature separation modeling with adaptive asynchronous identification achieved excellent terminal voltage tracking and internal temperature estimation over two extended cycles. The study also introduces and discusses the concept of parameter dispersion. Hani Sait [33] numerically studied thermoelectric cooling of a LIB using a cold side on the battery and a heat sink with triangular pin fins on the hot side. The triangular pin fins produced the highest pressure drop and output temperature compared to other fin designs. Yi et al. [34] studied a battery module with a double-sided thermoelectric device. They experimentally evaluated its heat dissipation and temperature regulation, then used analytical models to assess cooling and heating performance. The research demonstrated the effectiveness of the thermoelectric device for thermal management of battery modules. Pakrouh et al. [35] experimentally analyzed a novel liquid-cooled battery system with phase change material and a thermoelectric cooler. Unlike previous work, they used the phase change material to passively regulate the thermoelectric hot side temperature. They studied the effects of flow rate, cooler number, input power, and material type on performance. Higher flow rate, cooler number, and power reduced battery temperature. Pan et al. [36] developed a battery thermal management system using thermoelectric and liquid cooling. They compared heating modes to find the optimal operation, achieving efficient battery warm-up from −5 °C to 5 °C in 824 s with a specific thermoelectric system and fan voltage.

The examination of existing literature underscores the comprehensive investigation into thermoelectric technology's utilization for thermal regulation in battery systems. However, prevailing attention in most inquiries has centered on employing thermoelectric coolers to dissipate heat during battery discharge, frequently coupled with additional cooling methodologies like air cooling, phase change material, and liquid cooling. Traditionally, a thermoelectric device operates as a cooler by receiving an electric current, facilitating the transfer of heat from the hot side to the cold side, thereby cooling the battery. Yet, it possesses the dual capability of functioning as a generator, extracting wasted heat from the battery, depleting it from the cold side, and generating power. This dual functionality presents opportunities for both power generation from waste heat and the proficient temperature regulation of the battery. Consequently, this study proposes an innovative thermal management system for cylindrical LIBs, integrating an energy harvesting system based on a tubular thermoelectric generator (TTEG). Numerical simulations utilizing 3D finite element analysis with fully coupled physical fields are deployed to scrutinize dynamic behavior and assess the impact of various parameters on the electrical and thermal aspects of hybrid thermoelectric and battery systems. In this configuration, the TTEG comes into direct contact with the outer surface of the cylindrical battery. The primary objective is to evaluate the waste heat recovery capabilities of the TTEG for thermal management in the battery system. The study specifically delves into critical geometrical and operational parameters such as the battery discharge rate, the number of thermocouples (NTC) in the thermoelectric system, the heat transfer coefficient (HTC), and thermoelectric leg height to comprehensively evaluate the overall system performance. Notably, this research furnishes essential insights into optimizing waste heat recovery performance and enhancing the thermal management capabilities of TTEGs within the design framework of cylindrical battery systems. Through the augmentation of their performance across diverse applications, this study effectively addresses a significant void in prior research endeavors.

2. Numerical procedures

2.1. Solution domain and material properties

The Three-dimensional representation of the computational domain features a tubular configuration housing a thermoelectric generator affixed to a cylindrical battery as shown in Fig. 1. The TTEG consists of M rings, with each ring containing N sets of thermocouples. Each set within a ring includes both n-type and p-type thermocouples, intricately connected by curved copper electrical conductors. Adjacent to the thermoelectric generator, two alumina ceramic electrical insulators are affixed to its inner and outer surfaces. During the discharge phase, the cylindrical LIB serves as the thermal source, dissipating heat towards the inner facet of the TTEG. Simultaneously, the outer facet of the TTEG functions as a heat sink, making contact with the ambient air. The p-type and n-type constituents are crafted from low-temperature $Bi_{0.52}Sb_{1.48}Te_3$ and Bi_2Te_3 bismuth tellurides, respectively, given the consistently low operational temperature of the battery. Utilizing thermoelectric materials with lower temperature thresholds serves to optimize the overall efficiency of the system. The material characteristics of these p-type and n-type elements exhibit temperature-dependent variations, a feature intentionally incorporated to enhance the precision of the study. Polynomial expressions, incorporating temperature as a variable, are employed to model and predict the material properties of both elements, contributing to a more accurate estimation of the TTEG unit's outputs. Conversely, the properties of the alumina insulators, copper electrical conductors, and the battery remain constants in this analysis, simplifying the physical problem at hand. These constants provide a foundation for the study, allowing for a streamlined and more manageable calculation process. The Thermophysical properties of the LIB and thermoelectric

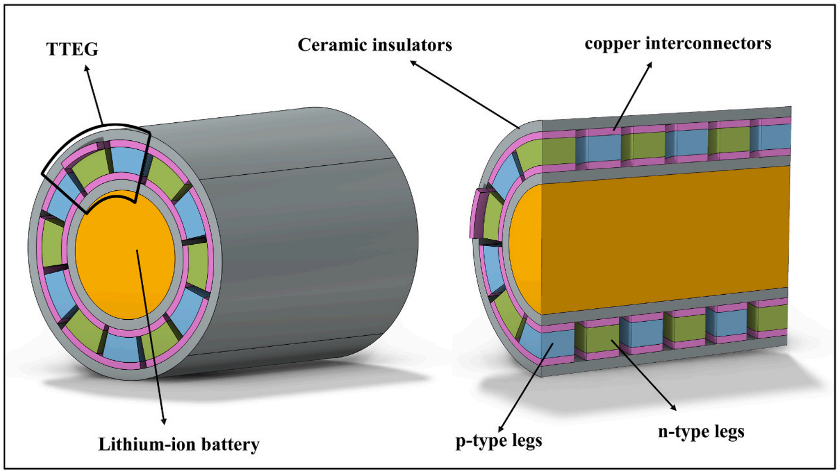

Fig. 1. 3D detailed view of the computational domain including the battery and TTEG.

elements are listed in Table 1. The geometric specification of the computational domain is shown in Fig. 2 and listed in Table 2. The battery sizes were chosen in accordance with the specifications detailed in Ref. [37], specifically focusing on the 18650 model. The specifications for the battery type, a maximum voltage of 3.7 V, a rated capacity of 2600 mAh, with a cathode material of LiNixCoyMnzO2 and an anode material of Graphite. Furthermore, the dimensions of the TTEG were established by considering the dimensions of the battery and specifications provided in the literature [38] as presented in Fig. 3.

2.2. Governing equations

Within the computational domain, there are two primary regions: the thermoelectric region and the battery region. In both of these zones, the heat transfer equation is addressed and can be expressed as follows [41]:

$$\rho C_p \frac{\partial T}{\partial t} + \nabla . q' = Q \tag{1}$$

Here, ρ and C_p denote the material's density and heat capacity, respectively, while Q represents the heat source. In the thermoelectric region, heat is produced as a result of Joule heating, which can be represented as [42]:

$$Q_j = J.E \tag{2}$$

Where J and E represent electric current density and electric field intensity, respectively, and can be described as follows [42]:

$$J = \sigma E + s \nabla T \tag{3}$$

$$E = -\nabla V \tag{4}$$

The governing equations relate the electric potential (V), conductivity (σ), and Seebeck coefficient (S). The model treats the battery cell as a homogeneous entity with uniform heat generation. The total heat generation rate of the LIBs is described as [40]:

$$Q_b = \frac{I_b}{V_b}\left(I_b R_b + T \frac{\partial V_{oc,b}}{\partial T}\right) \tag{5}$$

In this context, I_b represents the discharge current of battery, V_b denotes the battery volume, V_{oc} stands for the open circuit voltage of battery, $\frac{\partial V_{oc,b}}{\partial T}$ signifies the entropy coefficient, and R_b corresponds to the equivalent internal resistance of the battery.

2.3. Mathematical formulas

Key model parameters are explained here. The open circuit voltage from the input heat is:

$$V_{TEG} = S \Delta T \tag{6}$$

For a circuit with load resistor R_L and current I, the output power is:

$$I_{TEG} = \frac{S \Delta T}{R_L + R_{TEG}} \tag{7}$$

Table 1
Thermophysical properties of LIB and thermoelectric elements [39,40].

Bi_2Te_3 (p-type)	
$\lambda\ (Wm^{-2}K^{-1})$	$-3.31 \times 10^{-8}(T-T_0)^3 + 7.29 \times 10^{-5}(T-T_0)^2 - 3.79 \times 10^{-2}(T-T_0) + 7.12$
$R\ (\Omega m)$	$-7.60 \times 10^{-13}(T-T_0)^3 + 7.78 \times 10^{-10}(T-T_0)^2 - 1.93 \times 10^{-7}(T-T_0) + 1.8 \times 10^{-5}$
$\alpha\ (VK^{-1})$	$-2.96 \times 10^{-11}(T-T_0)^3 + 3.11 \times 10^{-8}(T-T_0)^2 - 1.08 \times 10^{-5}(T-T_0) + 1.48 \times 10^{-3}$
Bi_2Te_3 (n-type)	
$\lambda\ (Wm^{-2}K^{-1})$	$2.24 \times 10^{-8}(T-T_0)^3 + 7.09 \times 10^{-6}(T-T_0)^2 - 1.26 \times 10^{-2}(T-T_0) + 4.09$
$R\ (\Omega m)$	$-2.13 \times 10^{-13}(T-T_0)^3 + 1.42 \times 10^{-10}(T-T_0)^2 + 1.09 \times 10^{-8}(T-T_0) - 2.1 \times 10^{-6}$
$\alpha\ (VK^{-1})$	$1.46 \times 10^{-11}(T-T_0)^3 - 1.50 \times 10^{-8}(T-T_0)^2 + 5.14 \times 10^{-6}(T-T_0) - 8.12 \times 10^{-4}$
Copper interconnectors	
$\lambda\ (Wm^{-2}K^{-1})$	400
$\sigma\ (Sm)$	5.998×10^7
$\alpha\ (VK^{-1})$	6.5e-6
Alumina insulators	
$\lambda\ (Wm^{-2}K^{-1})$	30
$\sigma\ (Sm)$	1×10^{-16}
$\alpha\ (VK^{-1})$	0
Battery	
$\lambda\ (Wm^{-2}K^{-1})$	$\lambda_x = 0.9, \lambda_y = \lambda_z = 2.7$
$\rho_b\ (kgm^{-3})$	3000
$c_{p,b}\ (Jkg^{-1}K^{-1})$	900

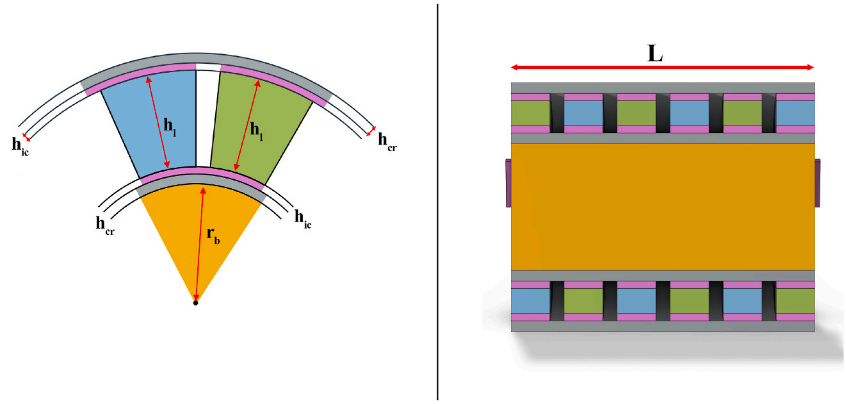

Fig. 2. Geometric specification of the battery and TTEG.

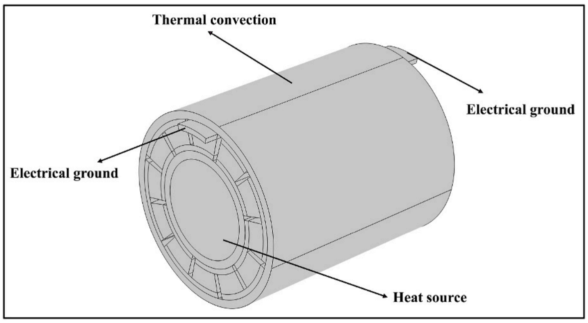

Fig. 3. A visual representation delineating the locations where boundary conditions and physics conditions are imposed on both the battery and the TTEG.

Table 2
Dimensions and parameters battery and TTEG

Partition Definition	Symbol	Dimension
TTEG		
height of PN legs	HL	4-12[mm]
height of ceramic insulators	h_{cr}	3 [mm]
height of copper interconnectors	h_{ic}	2 [mm]
number of thermocouples in each ring	N	6
number of rings	M	6
length of TTEG device	L	85 [mm]
Battery		
Radius of cylindrical battery	r_b	18 [mm]
Length of cylindrical battery	L	85 [mm]

$$P_{TEG} = \left(\frac{S\Delta T}{R_L + R_{TEG}}\right)^2 \times R_L \tag{8}$$

Incorporating the internal resistance denoted as R_{TEG} for the TTEG. Considering Q_h as the quantity of heat absorbed by the TTEG, the efficiency of conversion for the TTEG is expressed as:

$$\eta_{TEG} = \frac{P_{TEG}}{Q_h} \tag{9}$$

2.4. Boundary and zone conditions

The external surface of the TTEG interfaces with the surrounding air, engaging in convective heat transfer with a heat transfer coefficient denoted as (HTC) . The cylindrical battery experiences a volumetric heat source, Q_b. It is assumed that heat losses from all other surfaces of both the TTEG and the battery are negligible. The left copper block is subjected to a ground electrical boundary condition $(V = 0)$, while the right copper block is governed by an electrical potential boundary condition. All other surfaces maintain an electrical insulation boundary condition.

An empirical formulation, proposed by Li [43] and based on experimental measurements, is employed to compute the heat generation rate within a LIB over time, considering various C-rate conditions. The C-rate refers to the rate at which a battery is charged or discharged relative to its capacity. Specifically, it indicates how quickly a battery is charged or discharged compared to its nominal capacity, which is typically expressed in ampere-hours (Ah) [44]. The calculation of generated heat in the LIB is outlined as follows:

$$Q_b = A_1 t^6 + A_2 t^5 + A_3 t^4 + A_4 t^3 + A_5 t^2 + A_6 t + A_7 \tag{6}$$

Here, A1 to A7 are polynomial coefficients listed in Table 3.

2.5. Solution strategy

The 3D model equations were solved in COMSOL 6.1 using the finite element method to predict the electrical and thermal performance of the TTEG and battery. COMSOL is well-suited for interdisciplinary research due to its versatility. While other multi-physics software exists, COMSOL stands out for its capacity to swiftly and easily model systems governed by entirely unrelated fields [45]. An unstructured tetrahedral mesh was generated. A grid independence study verified the accuracy of the computational approach. Table 4 illustrates the changes in the maximum temperature of the battery and the highest thermoelectric voltage across three grid systems. The results exhibit a remarkable similarity across various mesh sizes. Nevertheless, the percentage of changes in the results compared to alterations in mesh size remains below 1 % for grid sizes exceeding 10000. Consequently, a mesh size of approximately 10000 is selected for the simulation. The meshing of the computational domain is demonstrated in Fig. 4.

A two-phase validation process was conducted due to the significant manufacturing costs. First, maximum battery temperatures at various discharge rates were validated against experiments by Li et al. [43] and simulations by Wu et al. [40]. Second, TTEG voltage versus temperature difference was compared to analytical results from Kaushik and Manikandan [46]. Fig. 5 (a) shows good agreement between experimental and simulated peak battery temperatures at 1C, 2C and 3C discharge. Fig. 5 (b) shows close alignment between simulated and analytical TTEG voltage versus temperature difference. The results validate the accuracy of the numerical approach for future investigations.

3. Results and discussion

This section delves into the examination of waste heat recovery and thermal management performance using a TTEG mounted on a cylindrical LIB. Key parameters analyzed include maximum battery temperature during discharge (T_{max}), TTEG output voltage (V_{TEG}), output power (P_{TEG}), and conversion efficiency (η_{TEG}). Subsequent sections further investigate the impacts of variations in several geometrical and operational parameters. These include the discharge rate of the battery, the number of thermocouples (NTC) in the thermoelectric system, the heat transfer coefficient (HTC), and the height of PN legs (HL). It is noteworthy that the conventional thermoelectric generator (TEG) employs interconnected n- and p-type elements, along with copper blocks featuring alumina insulators in a planar shape. In contrast, the elements of the TTEG adopt a tubular shape, making them suitable for application on curved surfaces. One surface of the TTEG makes contact with the battery heat source, while the outer surface serves to dissipate heat. Although some of the battery's thermal energy is lost from the outer surface of the TTEG, the TTEGs harness the remaining energy and convert it into voltage. The maximization of TTEG heat recovery stands as a pivotal factor in optimizing the overall performance of the device.

3.1. The effect of discharge rate

In this section, we investigate the influence of employing a TTEG on the thermal management of a cylindrical battery across various discharge rates. The T_{max} of the battery under various discharge rates were measured both without thermal management and with the integration of a TTEG. This comparison aimed to illustrate the advantages gained by employing TTEG in enhancing the thermal performance of the battery. As shown in Fig. 6 (a), the results indicate using a TTEG reduces the maximum battery temperature at all discharge rates. Consequently, it can be inferred that incorporating thermoelectric technology is advantageous for enhancing battery thermal management. According to the findings, as time elapses and the battery undergoes more discharge cycles, the reduction in the maximum temperature facilitated by TTEG becomes more pronounced. Utilizing a TTEG yields a maximum temperature decrease of 7.8 °C at 1C discharge rate and a substantial reduction of 21 °C at 2C discharge rate. This highlights the heightened effectiveness of TTEG for battery thermal management, especially at higher discharge rates.

On the other hand, considering waste heat recovery, it is evident from Fig. 6 (b) that the output voltage of the TTEG increases as the battery undergoes more discharges and generates more heat. Additionally, at higher discharge rates where more heat is generated, the output voltage of TTEG experiences a substantial growth. For instance, at 3C, TTEG produces a maximum output voltage of 0.24 V, while at 1C, the maximum thermoelectric voltage is 0.035 V, indicating a significant disparity in the maximum output voltage between these two discharge rates. This difference is attributed to the higher amount of heat generated in the battery at a discharge rate of 3C. Furthermore, Fig. 6 (c) illustrates the output power of the TTEG over time for various discharge rates of the battery. As anticipated, the

Table 3
Polynomial coefficients for heat generation during battery discharge [40].

Discharge rate	A_1	A_2	A_3	A_4	A_5	A_6	A_7
1C	4.9132e-16	−3.7742e-12	1.0679e-8	−1.3417e-5	0.0076	−2.2208	17151.7482
2C	1.2578e-13	−4.8310e-10	6.8347e-7	−4.2934e-4	0.1216	−17.7630	66623.3365
3C	3.2235e-12	−8.2542e-9	7.7851e-6	−3.2303e-3	0.6157	−59.9607	148414.7651

Table 4
Maximum temperature of battery and maximum thermoelectric voltage versus various mesh sizes

Number of meshes	Max T	Max V	Difference (%) T	Difference (%) V
4078	61.237	0.11567	−0.462138903	−1.03743408
10908	61.381	0.1163	−0.22645444	−0.49011178
17728	61.36	0.11648	−0.260756193	−0.334821429
29757	61.496	0.1168	−0.039026929	−0.059931507
43506	61.508	0.11686	−0.019509657	−0.008557248
62116	61.52	0.11687	0	0

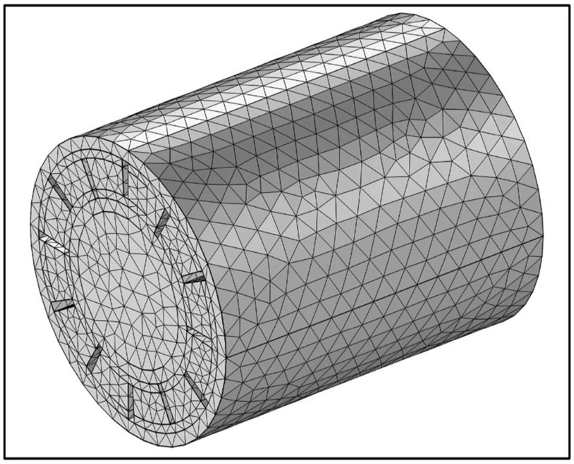

Fig. 4. Meshing of computational domain.

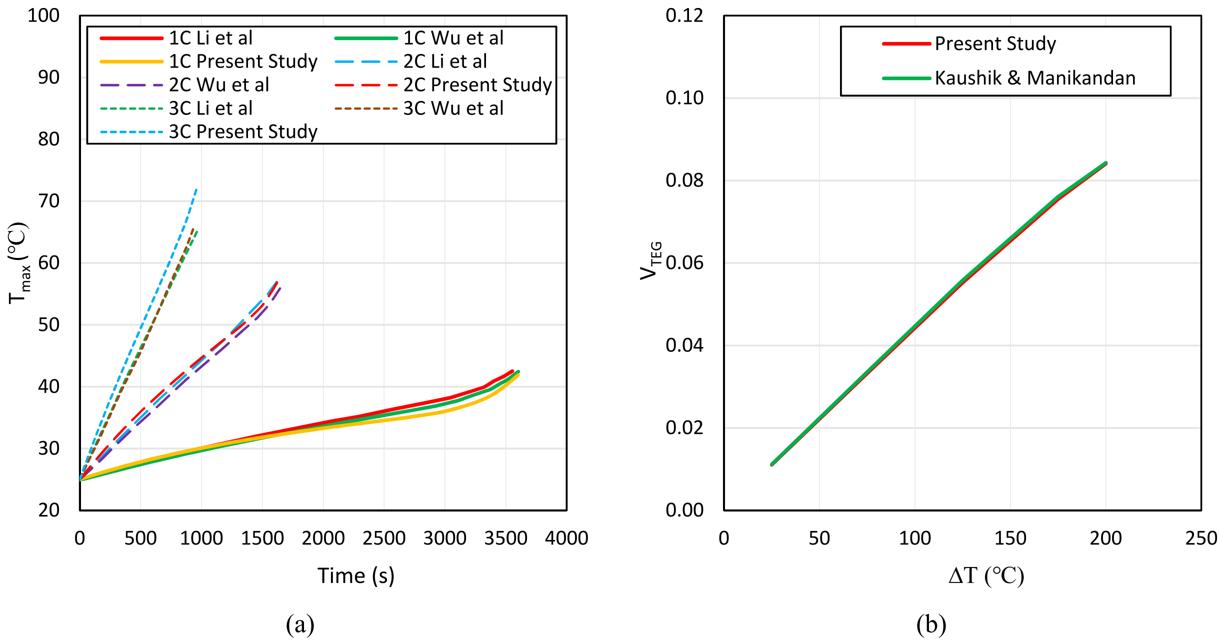

Fig. 5. Validation of numerical methods (a) maximum temperatures at various discharge rates of LIB (b) thermoelectric voltage versus temperature difference of TEG.

output power of the TTEG demonstrates a notable increase at higher discharge rates. This augmentation is attributed to the heightened heat generation within the battery, resulting in correspondingly higher voltage values. Moreover, the trends in output power demonstrate a substantial increase as the battery approaches full discharge. At a discharge rate of 3C, the TTEG demonstrated a power output of 0.071 W, in contrast to the maximum output power of 0.00135 W at 1C discharge rate. This underscores a significant

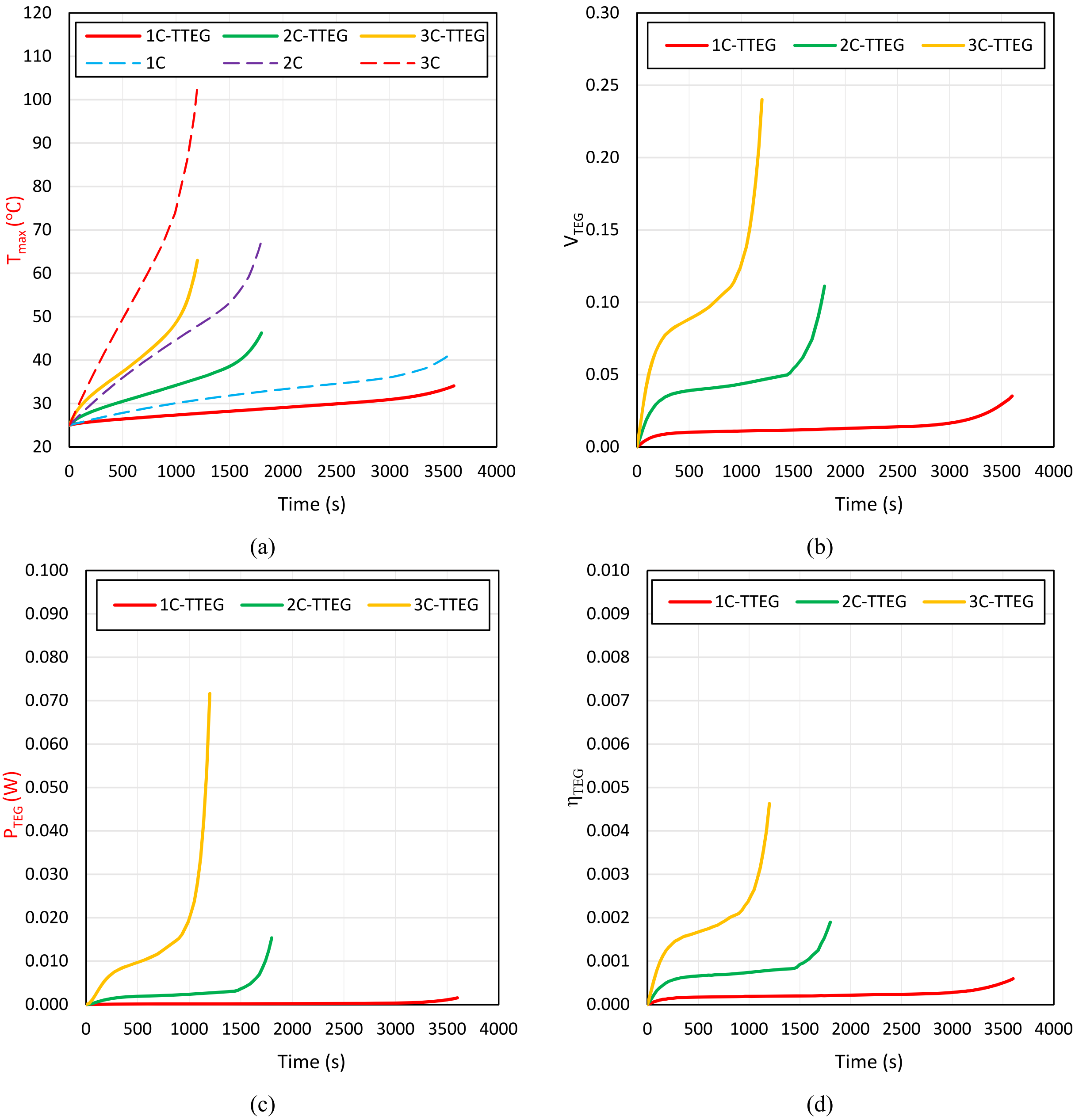

Fig. 6. The effect of discharge rate on different performance factors (a) maximum temperature of battery (b) output voltage of TTEG (c) output power of TTEG (d) conversion efficiency of TTEG ($\boldsymbol{NTC} = 64$, $\boldsymbol{HTC} = 5\ \boldsymbol{Wm^{-2}K^{-1}}$, $\boldsymbol{HL} = 7\boldsymbol{mm}$).

escalation in output power at higher discharge rates. The conversion efficiency of the TTEG is intricately linked to both the generated output power and the absorbed heat quantity. The efficiency of the thermoelectric conversion process is influenced by how effectively the TTEG can convert the thermal energy (heat) generated by the battery into electrical power. Therefore, a higher output power, combined with an optimal utilization of the absorbed heat, contributes to an enhanced conversion efficiency for the thermoelectric generator. As depicted in Fig. 6 (d), the trends of conversion efficiency of the TTEG over time, for various tested discharge rate values, closely mirror those observed in voltage and output power. As the battery approaches the end of discharge, the conversion efficiency of TTEG increases for all discharge rates. Similar to the patterns observed in output voltage and power, the conversion efficiency of TTEG is consistently higher for larger discharge rates, attributed to the larger amount of generated heat and the resulting higher output voltage and power.

3.2. The impact of the number of thermocouples (NTC)

This section delves into the influence of the quantity of thermocouples on the holistic performance of the system., encompassing both thermal management and waste heat recovery efficiency. The study considers five different TTEGs with varying thermocouple numbers, ranging from 16 to 144. In Fig. 7 (a), changes in the maximum battery temperature during discharge time at a 3C discharge rate are illustrated for different thermocouple configurations in the TTEG. The graph reveals that employing TTEG, regardless of the number of thermocouples, significantly reduces the maximum battery temperature. However, an intriguing observation is that as the number of thermocouples increases, there is a corresponding rise in the maximum battery temperature, particularly towards the end of the discharge cycle. This increase is attributed to the greater heat absorption from the battery with more thermocouples, resulting in higher voltage generated. The anticipated outcome is that a higher number of thermocouples would lead to a decrease in the maximum battery temperature due to increased heat absorption. However, the actual observation shows a growth in the maximum temperature. This seemingly contradictory result is explained by the fact that thermoelectric devices generate heat themselves, known as the Joule heat effect. Consequently, the reciprocal effect of increasing thermocouples becomes apparent. On one hand, more thermocouples enhance heat absorption, potentially lowering the battery temperature. On the other hand, the thermoelectric devices generate additional heat internally, contributing to an increase in the battery temperature. In conclusion, the temperature of the battery

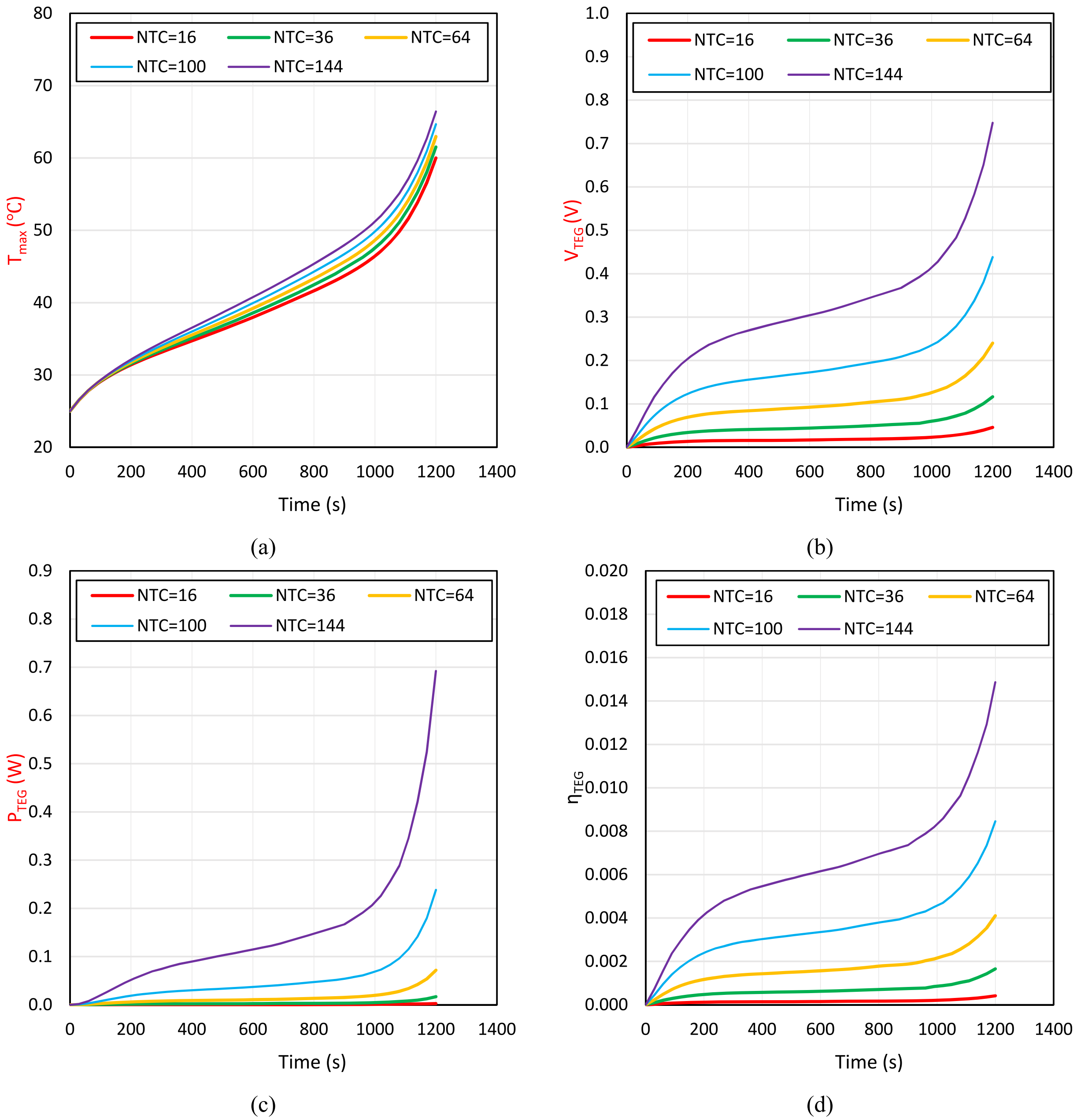

Fig. 7. The impact of NTC on different performance factors (a) maximum temperature of battery (b) output voltage of TTEG (c) output power of TTEG (d) conversion efficiency of TTEG ($C-rate = 3$, $HTC = 5\ Wm^{-2}K^{-1}$, $HL = 7mm$).

experiences a slight elevation with an increase in the number of thermocouples, as indicated by the observations. Additionally, as depicted in Fig. 7 (b), the augmentation of thermocouple numbers results in higher thermoelectric voltage values. This indicates a greater potential for waste heat recovery, as an increased number of thermocouples allows for the generation of more voltage. However, it's crucial to note that this potential is constrained by considerations of thermal management, as previously discussed. For example, increasing the number of thermocouples from 100 to 144 leads to a substantial up to 70 % increase in the voltage of the TTEG. The same trend is reflected in the output power, as illustrated in Fig. 7 (c). The findings reveal a noteworthy improvement in the output power of the TTEG as the number of thermocouples increases. This distinction becomes particularly pronounced towards the latter stages of the discharge cycle, where the battery generates more heat, leading to an augmented potential temperature difference between the two sides of the TTEG. The conversion efficiency of the TTEG aligns with the observed patterns in output voltage and power trends, as illustrated Fig. 7 (d). At higher numbers of thermocouples, the thermoelectric conversion efficiency is greater, underscoring that TTEGs with a larger number of thermocouples are more efficient from the perspective of waste heat recovery in LIBs. For instance, at its peak, the TTEG with 144 thermocouples exhibits a 75 % larger conversion efficiency compared to the TTEG with 100

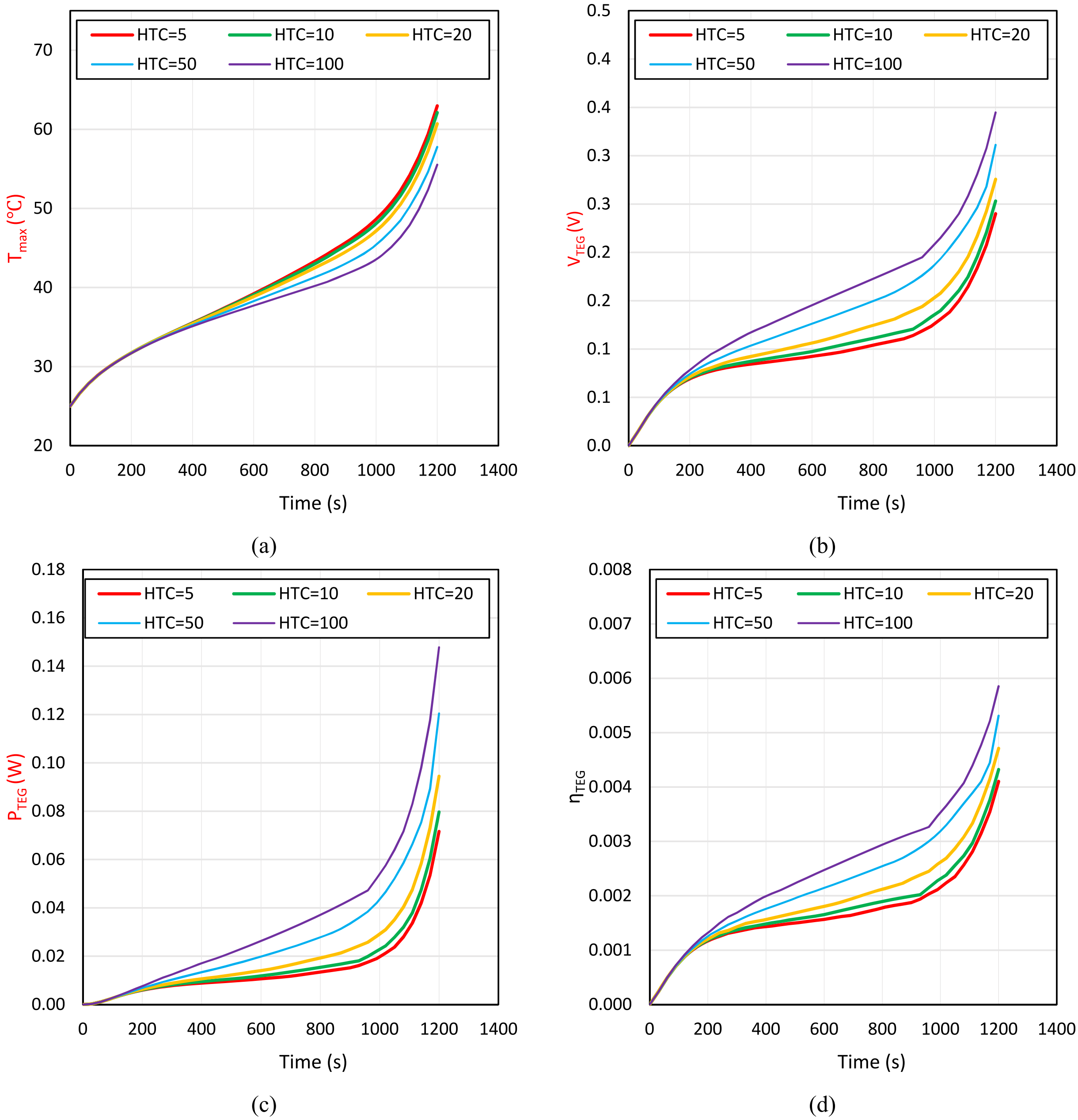

Fig. 8. The impact of HTC on different performance factors (a) maximum temperature of battery (b) output voltage of TTEG (c) output power of TTEG (d) conversion efficiency of TTEG ($\boldsymbol{NTC} = \mathbf{64}$, $\boldsymbol{C} - \boldsymbol{rate} = \mathbf{3}$, $\boldsymbol{HL} = \mathbf{7mm}$).

thermocouples.

3.3. The effect of heat transfer coefficient (HTC)

This section delves into the repercussions of the heat transfer coefficient (HTC) associated with the cold side of TTEG on the comprehensive functionality of the system, encompassing aspects of both thermal management and the efficiency of waste heat recovery. The analysis entails the examination of five distinct case studies, each featuring diverse HTC values ranging from 5 to 100. The primary objective of this inquiry is to assess how the HTC of air on the cold side of TTEG can influence the system's performance. This is crucial because the extent of heat transfer from the cold side of TTEG to the surrounding air can vary based on the airflow dynamics and the prevailing heat transfer regime. In Fig. 8 (a), variations in the maximum battery temperature during discharge time at a 3C discharge rate are depicted for different HTC values. The graph illustrates that the utilization of TTEG consistently diminishes the maximum battery temperature, irrespective of the HTC magnitude. The findings indicate that augmenting the HTC value has a positive impact on the TTEG's thermal management capability, leading to a reduction in the maximum battery temperature as the HTC increases. As observed in the results, the discrepancy in the maximum battery temperature among the tested scenarios becomes more pronounced towards the conclusion of the discharge cycle. For instance, at the peak, there is a substantial difference of 6.595 $^{\circ}C$ between the maximum battery temperature in the case with an HTC of 10 and the one with an HTC of 100. This underscores the heightened influence of HTC on thermal performance, particularly during critical phases of the discharge cycle. Moreover, considering the aspect of waste heat recovery, as illustrated in Fig. 8 (b), an escalation in the HTC leads to elevated thermoelectric voltage values. This signifies an enhanced capability for waste heat recovery, as an augmented HTC facilitates the generation of a higher voltage. In contrast to the impact discussed in the previous section regarding the augmentation of the number of thermocouples, elevating the HTC not only enhances thermal management capability but also concurrently increases the potential for waste heat recovery. The identical trend is evident in the output power, as depicted in Fig. 8 (c). The findings underscore a noteworthy improvement in the output power of the TTEG with a rise in the HTC. To exemplify, the escalation of the HTC from 10 to 20, particularly at the maximum amount the discharge cycle, results in a surge of 15.87 % in voltage and a substantial 34.28 % increase in output power. The efficiency of the TTEG, portrayed in Fig. 8 (d), aligns with the observed patterns in output voltage and power trends. At elevated HTC values, the thermoelectric conversion efficiency is notably higher, emphasizing that increased HTC results in a more efficient waste heat recovery in LIBs. To illustrate, at its zenith, the HTC of 20 showcases a 17.93 % higher conversion efficiency compared to the scenario with an HTC of 10.

3.4. The effect of the height of PN legs (HL)

In this segment, we investigate how varying the height of PN legs (HL) affects the overall system performance, including both thermal management and efficiency in recovering waste heat. The analysis encompasses five different hl values, ranging from 4 to 12 mm. Fig. 9 (a) depicts variations in the maximum battery temperature during discharge time at a 3C discharge rate for different heights of PN legs. The graph shows a consistent reduction in T_{max} with the utilization of TTEG, regardless of the magnitude of PN legs' heights. The results suggest that increasing the HL value positively influences the thermal management capability of TTEG, resulting in a decrease in the maximum battery temperature as HL increases. For example, at the peak, there is a significant difference of 2.66 °C between the maximum battery temperature in the case with an HL of 12 and the one with an HL of 4.

Furthermore, examining the aspect of waste heat recovery, as shown in Fig. 9 (b), an increase in HL leads to higher thermoelectric voltage values. This indicates an improved capability for waste heat recovery, as a higher HL facilitates the generation of increased voltage. In essence, raising the thermoelectric height results in a heightened temperature gradient between the two sides of the TTEG, leading to the growth of output voltage. The elevation of HL not only enhances thermal management capability but also augments the potential for waste heat recovery. A similar trend is evident in the output power, as depicted in Fig. 9 (c). The outcomes highlight a significant enhancement in the output power of the TTEG with an increase in HL due to the rise in output voltage. To illustrate, the escalation of HL from 4 to 12 mm, particularly at the maximum point in the discharge cycle, results in a surge of 182.77 % in voltage and a substantial 695 % increase in output power. The efficiency of the TTEG, as depicted in Fig. 9 (d), corresponds with the observed patterns in output voltage and power trends. At higher HL values, the thermoelectric conversion efficiency is significantly greater, underscoring that an increased HL leads to a more efficient waste heat recovery in LIBs. To illustrate, at its peak, the HL of 12 mm exhibits a 599 % higher conversion efficiency compared to the scenario with an HL of 4. In summary, augmenting the height of PN legs in the TTEG positively influenced thermal management, waste heat recovery, and overall system efficiency, providing valuable insights for optimizing the performance of thermoelectric devices in battery applications.

3.5. Conclusion

This research aimed to explore the efficacy of waste heat recovery and thermal management by implementing a Tubular Thermoelectric Generator (TTEG) on a cylindrical Lithium-ion Battery (LIB). The assessment covered critical parameters including the maximum battery temperature during discharge (T_{max}), the thermoelectric generator's output voltage (V_{TEG}), power output (P_{TEG}), and conversion efficiency (η_{TEG}). Key conclusions drawn from the study are as follows.

- Investigating the impact of TTEG on thermal regulation at various discharge rates consistently revealed reductions in the maximum battery temperature. TTEG implementation resulted in temperature reductions of up to 21 °C at higher discharge rates, underscoring its effectiveness in improving battery thermal management.
- Exploration of the influence of thermocouple numbers on TTEG performance yielded intriguing results. Contrary to expectations, an increase in the number of thermocouples led to a rise in the maximum battery temperature due to the Joule heat effect. However,

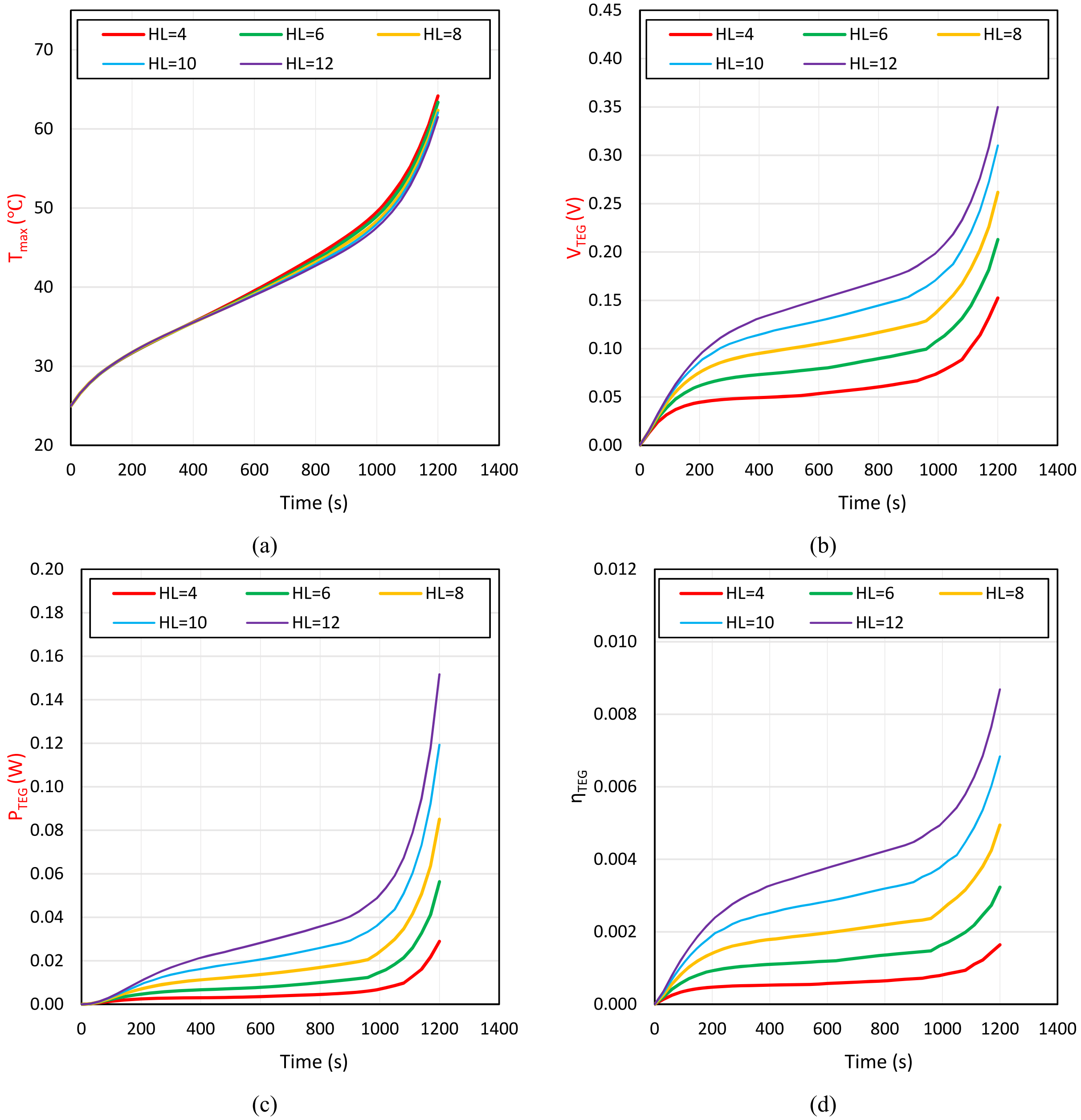

Fig. 9. The impact of height of PN legs (HL) on different performance factors (a) maximum temperature of battery (b) output voltage of TTEG (c) output power of TTEG (d) conversion efficiency of TTEG ($\boldsymbol{NTC} = 64$, $\boldsymbol{HTC} = 5\ \boldsymbol{Wm^{-2}K^{-1}}$, $\boldsymbol{C-rate} = 3$).

higher thermocouple numbers significantly enhanced waste heat recovery, output voltage, power, and conversion efficiency, particularly at larger discharge rates.

- Analysis of the heat transfer coefficient's impact on TTEG functionality demonstrated its critical role in thermal management. Increasing the HTC positively affected thermal performance, resulting in a substantial reduction in the maximum battery temperature. Moreover, elevated HTC contributed to higher thermoelectric voltage, power, and conversion efficiency, emphasizing its dual role in enhancing waste heat recovery. Boosting HTC from 10 to 20, especially during maximum discharge, results in a 15.87 % surge in voltage and a significant 34.28 % increase in output power.
- Assessing the effect of varying the height of PN legs on TTEG performance consistently showed reductions in maximum battery temperature, reinforcing TTEG's effectiveness in thermal management. Furthermore, increasing the leg height positively influenced waste heat recovery, leading to higher thermoelectric voltage, power, and conversion efficiency, thereby optimizing system efficiency.

Overall, the study highlights that TTEG integration enhances thermal management and waste heat recovery in LIBs. Each parameter - discharge rate, thermocouple number, heat transfer coefficient, and PN legs' height - plays a unique role in improving TTEG effectiveness, providing valuable insights for optimizing thermoelectric devices in battery applications.

CRediT authorship contribution statement

Xiao Zhou: Supervision, Conceptualization. **Azher M Abed:** Formal analysis, Data curation. **Rishabh Chaturvedi:** Methodology, Investigation. **Barno Sayfutdinovna Abdullaeva:** Writing – review & editing, Resources. **Ali Shawabkeh:** Writing – review & editing, Writing – original draft, Validation. **Yasser Fouad:** Project administration, Funding acquisition. **Fahid Riaz:** Writing – review & editing, Writing – original draft, Investigation.

Declaration of competing interest

The authors declare that they have no known competing financial interests or personal relationships that could have appeared to influence the work reported in this paper.

Data availability

The authors do not have permission to share data.

Acknowledgement

The authors extend their appreciation to the Reserachers Supporting Project number (RSPD2024R698), King Saud University, Riyadh, Saudi Arabia for funding this research work. The study was funded by Al -Mustaqbal University (project No: 2/2024).

References

[1] Y. Zhou, B. Wang, Z. Ling, Q. Liu, X. Fu, Y. Zhang, et al., Advances in ionogels for proton-exchange membranes, Sci. Total Environ. 921 (2024) 171099, https://doi.org/10.1016/j.scitotenv.2024.171099.
[2] Z. Ma, J. Zhao, L. Yu, M. Yan, L. Liang, X. Wu, et al., A review of energy supply for biomachine hybrid robots, Cyborg Bionic Syst 4 (2023) 53, https://doi.org/10.34133/cbsystems.0053.
[3] L. Lu, W. Wu, Y. Gao, C. Pan, X. Yu, C. Zhang, Z. Jin, Study on current discrepancy and redistribution of HTS non-insulation closed-loop coils during charging/discharging and subsequent transient process toward steady-state operation, Supercond Sci Technol 35 (9) (2022) 95001, https://doi.org/10.1088/1361-6668/ac7dfe.
[4] S. Xue, J. Shang, X. Pu, H. Cheng, L. Zhang, C. Wang, Y. Tang, Dual anionic doping strategy towards synergistic optimization of Co9S8 for fast and durable sodium storage, Energy Storage Mater 55 (2023) 33–41. https://doi.org/10.1016/j.ensm.2022.11.040.
[5] Dipan Arora, Alaa El-Sharkawy, Satyam Panchal, Development of time-temperature analysis algorithm for estimation of lithium-ion battery useful life, WCX SAE World Congr. Exp., SAE International (2024), https://doi.org/10.4271/2024-01-2191.
[6] Junran Chen, Phillip Kollmeyer, Satyam Panchal, Yasaman Masoudi, Oliver Gross, Ali Emadi, Sequence training and data shuffling to enhance the accuracy of recurrent neural network based battery voltage models, in: WCX SAE World Congr. Exp., SAE International, 2024, https://doi.org/10.4271/2024-01-2426.
[7] X. Bai, M. Xu, Q. Li, L. Yu, Trajectory-battery integrated design and its application to orbital maneuvers with electric pump-fed engines, Adv Sp Res 70 (2022) 825–841, https://doi.org/10.1016/j.asr.2022.05.014.
[8] M.K. Tufail, P. Zhai, M. Jia, N. Zhao, X. Guo, Design of solid electrolytes with fast ion transport: computation-driven and practical approaches, Energy Mater Adv 4 (2023), https://doi.org/10.34133/energymatadv.0015.
[9] H. Lü, X. Chen, Q. Sun, N. Zhao, X. Guo, Uniform garnet nanoparticle dispersion in composite polymer electrolytes, Acta Phys Chim Sin 40 (3) (2024) 2305016, https://doi.org/10.3866/PKU.WHXB202305016.
[10] N. Ghaeminezhad, Z. Wang, Q. Ouyang, A Review on lithium-ion battery thermal management system techniques: a control-oriented analysis, Appl. Therm. Eng. 219 (2023) 119497, https://doi.org/10.1016/j.applthermaleng.2022.119497.
[11] S. Vashisht, D. Rakshit, S. Panchal, M. Fowler, R.A. Fraser, Quantifying the effects of temperature and depth of discharge on Li-ion battery heat generation: an assessment of resistance models for accurate thermal behavior prediction, ECS Meet Abstr (2023).
[12] M.-K. Tran, A. DaCosta, A. Mevawalla, S. Panchal, M. Fowler, Comparative study of equivalent circuit models performance in four common lithium-ion batteries: LFP, NMC, LMO, NCA, Batteries 7 (2021), https://doi.org/10.3390/batteries7030051.
[13] X. Zhang, Y. Tang, F. Zhang, C.-S. Lee, A novel aluminum–graphite dual-ion battery, Adv. Energy Mater. 6 (2016) 1502588, https://doi.org/10.1002/aenm.201502588.
[14] M. Wang, C. Jiang, S. Zhang, X. Song, Y. Tang, H.-M. Cheng, Reversible calcium alloying enables a practical room-temperature rechargeable calcium-ion battery with a high discharge voltage, Nat. Chem. 10 (2018) 667–672, https://doi.org/10.1038/s41557-018-0045-4.
[15] Y. Wei, B. Tang, X. Liang, F. Zhang, Y. Tang, An ultrahigh-mass-loading integrated free-standing functional all-carbon positive electrode prepared using an architecture tailoring strategy for high-energy-density dual-ion batteries, Adv Mater 35 (2023) 2302086, https://doi.org/10.1002/adma.202302086.
[16] A. Maiorino, C. Cilenti, F. Petruzziello, C. Aprea, A review on thermal management of battery packs for electric vehicles, Appl. Therm. Eng. 238 (2024) 122035, https://doi.org/10.1016/j.applthermaleng.2023.122035.
[17] J. Xiang, J. Liu, W. Yang, X. Wei, P. Li, Z. Chen, et al., Development of novel thermal diode based on improved check valve and modified wick structure, Int. J. Therm. Sci. 200 (2024) 108977, https://doi.org/10.1016/j.ijthermalsci.2024.108977.
[18] R. Youssef, T. Kalogiannis, H. Behi, A. Pirooz, J. Van Mierlo, M. Berecibar, A comprehensive review of novel cooling techniques and heat transfer coolant mediums investigated for battery thermal management systems in electric vehicles, Energy Rep. 10 (2023) 1041–1068, https://doi.org/10.1016/j.egyr.2023.07.041.
[19] H. Najafi Khaboshan, F. Jaliliantabar, A.A. Abdullah, S. Panchal, A. Azarinia, Parametric investigation of battery thermal management system with phase change material, metal foam, and fins; utilizing CFD and ANN models, Appl. Therm. Eng. 247 (2024) 123080, https://doi.org/10.1016/j.applthermaleng.2024.123080.
[20] M.S. Patil, J.-H. Seo, S. Panchal, S.-W. Jee, M.-Y. Lee, Investigation on thermal performance of water-cooled Li-ion pouch cell and pack at high discharge rate with U-turn type microchannel cold plate, Int J Heat Mass Transf 155 (2020) 119728, https://doi.org/10.1016/j.ijheatmasstransfer.2020.119728.
[21] Virendra Talele, Mahesh Suresh Patil, Uğur Moralı, Satyam Panchal, Roydon Fraser, Michael Fowler, et al., Battery thermal runaway preventive time delay strategy using different melting point phase, Change Materials (2023), https://doi.org/10.4271/14-13-03-0017.

[22] J. Zhu, R. Chaturvedi, Y. Fouad, I. Albaijan, N. Juraev, L.H. Alzubaidi, et al., A numerical modeling of battery thermal management system using nano-enhanced phase change material in hot climate conditions, Case Stud. Therm. Eng. 58 (2024) 104372, https://doi.org/10.1016/j.csite.2024.104372.

[23] H. Lin, F. Aldawi, S.A. Reda, Z.R. Abdulghani, S. Asaadi, H. Sadighi Dizaji, Economic cost and thermal efficiency analysis of porous-minichannel heat exchanger for thermoelectric generator, Appl. Therm. Eng. 213 (2022) 118653, https://doi.org/10.1016/j.applthermaleng.2022.118653.

[24] Y. Lyu, A.R.M. Siddique, S.H. Majid, M. Biglarbegian, S.A. Gadsden, S. Mahmud, Electric vehicle battery thermal management system with thermoelectric cooling, Energy Rep. 5 (2019) 822–827, https://doi.org/10.1016/j.egyr.2019.06.016.

[25] H. Li, X. Wang, A. Saini, Y. Zhu, Y.-P. Wang, State of charge estimation for lithium-ion battery models based on a thermoelectric coupling model, Int. J. Electrochem. Sci. 15 (2020) 3807–3824, https://doi.org/10.20964/2020.05.41.

[26] H. Alhumade, E. Almatrafi, M. Rawa, A.S. El-Shafay, C. Qi, Y. Khetib, Numerical study of simultaneous use of non-Newtonian hybrid nano-coolant and thermoelectric system in cooling of lithium-ion battery and changes in the flow geometry, J. Power Sources 540 (2022) 231626, https://doi.org/10.1016/j.jpowsour.2022.231626.

[27] L. Jiang, H. Zhang, J. Li, P. Xia, Thermal performance of a cylindrical battery module impregnated with PCM composite based on thermoelectric cooling, Energy 188 (2019) 116048, https://doi.org/10.1016/j.energy.2019.116048.

[28] G. Liao, K. Jiang, F. Zhang, J. E, L. Liu, J. Chen, et al., Thermal performance of battery thermal management system coupled with phase change material and thermoelectric elements, J. Energy Storage 43 (2021) 103217, https://doi.org/10.1016/j.est.2021.103217.

[29] Y. Lyu, A.R.M. Siddique, S.A. Gadsden, S. Mahmud, Experimental investigation of thermoelectric cooling for a new battery pack design in a copper holder, Results Eng 10 (2021) 100214, https://doi.org/10.1016/j.rineng.2021.100214.

[30] J. Tu, C. Qi, S. Zhang, Z. Tang, Comprehensive thermal-hydraulic performance and thermoelectric conversion efficiency of bionic battery waste heat recovery system, J. Energy Storage 48 (2022) 104039, https://doi.org/10.1016/j.est.2022.104039.

[31] X. Cui, T. Hu, Robust predictive thermal management strategy for lithium-ion battery based on thermoelectric cooler, Appl. Therm. Eng. 221 (2023) 119833, https://doi.org/10.1016/j.applthermaleng.2022.119833.

[32] H. Shi, S. Wang, C. Fernandez, C. Yu, W. Xu, B.E. Dablu, et al., Improved multi-time scale lumped thermoelectric coupling modeling and parameter dispersion evaluation of lithium-ion batteries, Appl. Energy 324 (2022) 119789, https://doi.org/10.1016/j.apenergy.2022.119789.

[33] H. Sait, Cooling a plate lithium-ion battery using a thermoelectric system and evaluating the geometrical impact on the performance of heatsink connected to the system, J. Energy Storage 52 (2022) 104692, https://doi.org/10.1016/j.est.2022.104692.

[34] Z. Yi, P. Wei, H. Zhang, H. Sun, S. Zeng, H. Yu, Wide range temperature thermal performance of power battery module with double-sided thermoelectric device system with high energy efficiency, Appl. Therm. Eng. 227 (2023) 120375, https://doi.org/10.1016/j.applthermaleng.2023.120375.

[35] R. Pakrouh, A.A. Ranjbar, M.J. Hosseini, M. Rahimi, Thermal management analysis of new liquid cooling of a battery system based on phase change material and thermoelectric cooler, Appl. Therm. Eng. 231 (2023) 120925, https://doi.org/10.1016/j.applthermaleng.2023.120925.

[36] Y. Pan, A. Tang, Z. Liu, C. Shan, Experimental analysis of power battery preheating system based on thermoelectric elements, Appl. Therm. Eng. 230 (2023) 120860, https://doi.org/10.1016/j.applthermaleng.2023.120860.

[37] L. Li, L. Ling, Y. Xie, W. Zhou, T. Wang, L. Zhang, et al., Comparative study of thermal management systems with different cooling structures for cylindrical battery modules: side-cooling vs. terminal-cooling, Energy 274 (2023) 127414, https://doi.org/10.1016/j.energy.2023.127414.

[38] S. Asaadi, S. Khalilarya, S. Jafarmadar, Numerical study on the thermal and electrical performance of an annular thermoelectric generator under pulsed heat power with different types of input functions, Energy Convers. Manag. 167 (2018), https://doi.org/10.1016/j.enconman.2018.04.085.

[39] M. Li, H.S. Dizaji, S. Asaadi, F. Jarad, A.E. Anqi, M. Wae-hayee, Thermo-economic, exergetic and mechanical analysis of thermoelectric generator with hollow leg structure; impact of leg cross-section shape and hollow-to-filled area ratio, Case Stud. Therm. Eng. 27 (2021) 101314, https://doi.org/10.1016/j.csite.2021.101314.

[40] C. Wu, J. Ni, X. Shi, R. Huang, A new design of cooling plate for liquid-cooled battery thermal management system with variable heat transfer path, Appl. Therm. Eng. 239 (2024) 122107, https://doi.org/10.1016/j.applthermaleng.2023.122107.

[41] A.H. Vakilzadeh, A.B. Sarvestani, K. Javaherdeh, R. Kamali, S. Panchal, Heat transfer and fluid flow in a PCM-filled enclosure: effect of heated wall configuration, J. Energy Storage 87 (2024) 111448, https://doi.org/10.1016/j.est.2024.111448.

[42] S. Asaadi, S. Khalilarya, S. Jafarmadar, A thermodynamic and exergoeconomic numerical study of two-stage annular thermoelectric generator, Appl. Therm. Eng. 156 (2019) 371–381, https://doi.org/10.1016/j.applthermaleng.2019.04.058.

[43] L. Tao, Study on Thermal Effects of Lithium-Ion Battery in Electric Vehicle and Battery Package Dissipation Structural Optimization, Chongqing Univ, 2013, pp. 13–47.

[44] G.L. Plett, Battery Management Systems, Volume II: Equivalent-Circuit Methods, Artech House, 2015.

[45] C. Zhu, Optimizing and using AI to study of the cross-section of finned tubes for nanofluid-conveying in solar panel cooling with phase change materials, Eng. Anal. Bound. Elem. 157 (2023) 71–81, https://doi.org/10.1016/j.enganabound.2023.08.018.

[46] S.C. Kaushik, S. Manikandan, The influence of Thomson effect in the energy and exergy efficiency of an annular thermoelectric generator, Energy Convers. Manag. 103 (2015) 200–207, https://doi.org/10.1016/j.enconman.2015.06.037.